

Regularized scheme of time evolution tensor network algorithms

Li-Xiang Cen*

Center of Theoretical Physics, College of Physics, Sichuan University, Chengdu 610065, China

(Dated: August 9, 2022)

Regularized factorization is proposed to simulate time evolution for quantum lattice systems. Transcending the Trotter decomposition, the resulting compact structure of the propagator indicates a high-order Baker-Campbell-Hausdorff series. Regularized scheme of tensor network algorithms is then developed to determine the ground state energy for spin lattice systems with Heisenberg or Kitaev-type interactions. Benchmark calculations reveal two distinct merits of the regularized algorithm: it has stable convergence, immune to the bias even in applying the simple update method to the Kitaev spin liquid; contraction of the produced tensor network can converge rapidly with much lower computing cost, relaxing the bottleneck to calculate the physical expectation value.

Tensor network (TN) and the built numerical algorithms on it have earned great success in the simulation of quantum many-body systems [1, 2], providing deep insights into relevant physics, e.g., the ground state (GS) property and dynamics for gapped systems [3–6], the scaling behavior for critical systems [7–10], and the strongly correlated physics for frustrated systems [11–15]. For one-dimensional (1D) quantum lattice systems, the matrix product state (MPS), which originally recognized as the target state of the density matrix renormalization group algorithm [16–18], is the basis of the infinite time evolving block decimation (iTEBD) algorithm [19, 20]. The latter allows for direct simulations of both static and dynamic properties of spin chains in the thermodynamical limit and has boosted vastly the development of the TN-based algorithm from the 1D to high-dimensional lattices and from the spin system to interacting fermionic systems [21–24]. The two-dimensional (2D) TN state, known as the projected entangled pair state (PEPS) [25, 26] and its variant the projected entangled simplex state (PESS) [27], are natural generalizations of the MPS and have become standard tools for capturing the physics of the 2D strongly correlated quantum systems [28–31].

Frustrated spin systems can give rise to rich phases of quantum matter and have attracted intensive interests in past decades [32–37]. Due to strong quantum fluctuations, a particular puzzle associated with the study of frustrated models, which arouses further the fascination of wider numerical investigation to them, is that the results obtained by different methods sometimes cannot reach consensus—paradigms including the cross-coupled antiferromagnetic spin ladder [38–41] and the notorious kagome antiferromagnet [34, 42–49]. At this point, the Kitaev honeycomb model (KHM) [50] offers an intriguing litmus test and research object as well for the numerical methods in view that: (1) the pure KHM is analytically solvable; (2) it exhibits gapless and gapped Kitaev spin liquid phases with fractionalized excitations; (3) the numerical study is necessarily required when competing

interactions, say, the isotropic Heisenberg interactions and/or the symmetric anisotropic Γ interactions are superimposed on the KHM [51–55].

Although the variational approach [56] shows that the 2D TN wave function can capture precisely the features of the Kitaev spin liquid phase, previous studies based on the imaginary time evolution TN algorithm couldn't achieve satisfactory results for the KHM [53]: the full update infinite PEPS calculation suffers from a bias with which the GS symmetry of null magnetization is not guaranteed, while the simple update method is not able to yield stable convergence from randomly given initial states. In this paper we will propose a regularized scheme to implement the TN algorithm in which the time evolution operator is split into a more compact structure instead of the Trotter-Suzuki formula [57]. It turns out that the regularized TN algorithm is not only able to yield more precise results for 1D lattice systems, but also its 2D extension can produce reliable non-magnetized outcomes of spin liquid phases for the KHM.

One computational bottleneck of the 2D TN algorithm is the contraction of the full TN which is required in order to obtain the physical expectation value. Since the approximation of the contracting process does not meet the variational principle, the truncation error induced at this step should be much less than that of the TN wave function so as to warrant the obtained GS energy to be the upper bound of the exact one. As this error is visible from the convergence character, early studies on the PEPS and PESS display that to reach high accuracy for the contraction is computationally very expensive [58]. Remarkably, for the states produced by the regularized TN algorithm on the honeycomb lattice with either the Kitaev-type or the Heisenberg interactions, the accuracy of the contraction is shown to be dramatically improved even using less computational resources, which significantly helps to retain the variational principle and relaxes the bottleneck of the TN algorithm in its application.

Let us start by considering the time evolution operator e^{-itH} , or the Gibbs operator $e^{-\beta H}$, of an infinite quantum spin chain, where H is a Hamiltonian with local interactions and β accounts for the inverse temperature. We divide H into \mathcal{N} copies of linked size- L blocks, $H = \sum_{k=1}^{\mathcal{N}} (H_L^{[k]} + v^{k,k+1})$, in which $v^{k,k+1}$ denotes the

* lixiangcen@scu.edu.cn

interblock coupling and the periodic boundary condition has been assumed. The propagator generated by the free terms, i.e., $H_0 \equiv \sum_k H_L^{[k]}$ of all disconnected blocks, constitutes a piece-wise local operator $[U_L(\tau)]^{\otimes \mathcal{N}}$ with $U_L(\tau) = e^{-\tau H_L}$. In the case that the block size L is considerably large or τ is small enough, the whole evolution generated by H can be simulated by the following decomposition

$$e^{-\tau H} = [\bar{U}_L(\tau)]^{\otimes \mathcal{N}} \times [U_L(\tau)]^{\otimes \mathcal{N}}. \quad (1)$$

The operator in the second layer, $\bar{U}_L(\tau)$, which acts on the two coarse-grained sublattices of (s_r, s_l) —the right half of the k th block and the left half of the $(k+1)$ th block, is the key ingredient that the present scheme would outperform the Trotter decomposition. It is constructed through an inward algorithm, i.e., resorting to the propagators generated by a pair of length- L blocks that have the same boundary condition, but one has and the other hasn't the intermediate coupling [see Fig. 1(a)]. Specifically, the two block Hamiltonians with open boundary read as $H_L = h_l + v^{l,r} + h_r$ and $h_l + h_r$, which give rise to an ‘‘open prescription’’ of the regularized scheme to construct the operator [59]

$$\bar{U}_L^{(1)}(\tau) = e^{-\tau H_L} e^{\tau(h_l+h_r)}. \quad (2)$$

Alternatively, one can make use of the ‘‘periodic prescription’’, exploiting propagators generated by two Hamiltonians with connected boundary: $H_L^p \equiv H_L + v^{r,l}$ and $H_L^\circ \equiv H_L^p - v^{l,r}$, to construct

$$\bar{U}_L^{(2)}(\tau) = e^{-\tau H_L^p} e^{\tau H_L^\circ}. \quad (3)$$

As the superiority of these two regularized prescriptions will be demonstrated later on by numerical calculations, the rationality of them can be briefly interpreted by rewriting the propagator $e^{-\tau H}$ as

$$\begin{aligned} e^{-\tau H} &= e^{-\tau H} e^{\tau H_0} e^{-\tau H_0} \\ &= e^{-\sum_{k=1}^{\mathcal{N}} V^{k,k+1}} \times e^{-\tau H_0}, \end{aligned} \quad (4)$$

in which $V^{k,k+1}$ denotes the collection of terms of the Baker-Campbell-Hausdorff (BCH) series. It involves the coupling term $v^{k,k+1}$, the commutator between $v^{k,k+1}$ and H_0 : $[H, H_0] = \sum_k [v^{k,k+1}, H_0]$, and the resulting nestings. The range of each $V^{k,k+1}$ will successively increase but be restricted by the order of the BCH expansion. If this range does not exceed the length L under a limited expanding order, the operator of the second layer manifests a piece-wise structure and every local piece can be simulated by both of $\bar{U}_L^{(1)}(\tau)$ and $\bar{U}_L^{(2)}(\tau)$ [60].

It is readily seen that the lowest order of the regularized factorization, the case of $L = 2$, recovers the Trotter-Suzuki formula since the corresponding sublattices have trivial structure and $H_L = v^{l,r}$. Its high-order scheme with $L \geq 4$ then illuminates an improved way to implement the iterative operations for the iTEBD and, with its natural generalizations, for the PEPS on high-dimensional quantum lattice systems. To be specific, let

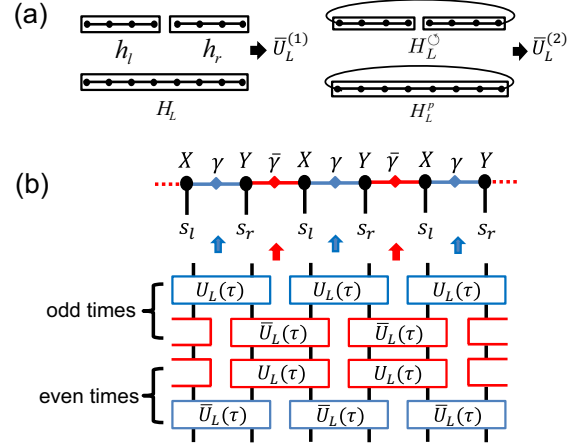


FIG. 1. Regularized scheme to split the time evolution operator for 1D quantum lattices. (a) Block Hamiltonians with different configurations via which the operators $\bar{U}_L^{(1)}(\tau)$ and $\bar{U}_L^{(2)}(\tau)$ are constructed [see Eqs. (2) and (3)]. (b) ‘‘Gate’’ operations of $U_L(\tau)$ and $\bar{U}_L(\tau)$ on (s_l, s_r) or (s_r, s_l) of the coarse-grained sites, and a staggered manner to perform the iteration is illustrated. The local tensor X (Y) of the MPS has one physical index and two virtual indices and γ ($\bar{\gamma}$) accounts for the diagonal matrix.

$|\psi_0\rangle$ be a randomly given initial state and set the imaginary time evolution $e^{-\beta H} = (e^{-\tau H})^M$ with $M \equiv \beta/\tau$ the Trotter number. One applies either the open or the periodic prescription described in Eqs. (1)-(3) to perform $e^{-\tau H}$ iteratively, so that the projected state $e^{-\beta H}|\psi_0\rangle$ converges to the GS in the limit $\beta \rightarrow \infty$. Regularized version of the iTEBD (rTEBD) is readily built in which the update scheme of the iTEBD is retained but the representative tensors X^{s_l} and Y^{s_r} of the MPS [see Fig. 1 (b)] are now defined on the coarse-grained sites with enlarged spin dimension $d \rightarrow d^{\frac{L}{2}}$.

In detail, the rTEBD algorithm with various block size L (referred as rTEBD- L) is applied to obtain the GS $|\psi\rangle$ for the infinite 1D Heisenberg antiferromagnets (HAF) $H = \sum_i \mathbf{S}_i \cdot \mathbf{S}_{i+1}$ with $s = \frac{1}{2}$ and $s = 1$. Below are some particular points worthy to mention. (1) The algorithm preserves only the translational symmetry of L sites. A staggered manner to implement the iteration [see Fig. 1 (b)], that is, imposing the operators $U_L(\tau)$ and $\bar{U}_L(\tau)$ successively on (s_l, s_r) and (s_r, s_l) in every odd time but imposing the former on (s_r, s_l) and the latter on (s_l, s_r) in every even time (recovering the so-called ‘‘second-order Trotter decomposition’’ as $L = 2$), is helpful to restore the translational symmetry of $L/2$ -site shifts. (2) The GS energy per site is given by $e_g = e_L/L$ with $e_L \equiv \langle \psi | (H_L + v^{k,k+1}) | \psi \rangle / \langle \psi | \psi \rangle$. Numerical calculation displays that the accuracy of e_L is noticeably better than that of the bulk $\langle H_L \rangle$ and of the coupling $\langle v^{k,k+1} \rangle$, separately. (3) In all calculations of the rTEBD- L shown in Table I, the Trotter error is made negligibly small (down to 10^{-8}). So it is safe to conclude that the

TABLE I. GS energies of infinite HAF chains given by the rTEBD algorithm. For references, the exact value of the $s = \frac{1}{2}$ model is $\frac{1}{4} - \ln 2 \approx -0.4431472$; the value of the $s = 1$ model to the first 12 digits is -1.40148403897 [17].

e_g	rTEBD-2	rTEBD-4	rTEBD-6	rTEBD-8
$s = 1$				
$\mathcal{D} = 20$	-1.4014590	-1.4014702	-1.4014740	-1.4014764
$\mathcal{D} = 30$	-1.4014835	-1.4014838	-1.4014838	-1.4014839
$s = \frac{1}{2}$				
$\mathcal{D} = 30$	-0.4431382	-0.4431399	-0.4431411	-0.4431418
$\mathcal{D} = 40$	-0.4431430	-0.4431438	-0.4431442	-0.4431446

visible improvement of the results obtained by the high-order rTEBD- L with the same bond dimension \mathcal{D} is not owing to the reduction of the Trotter error, but the regularized algorithm takes more correlations into account hence is able to suppress the truncation error induced by the approximation of the mean-field-like environment.

The extra cost for the rTEBD with increasing L is the memory resource that is proportional to the square of the coarse-grained spin dimension $d^{\frac{L}{2}}$. On the other hand, alteration to the time cost should concern comprehensively the cubic-power relation with the spin dimension $d^{\frac{L}{2}}$ and the relaxation of the step size τ in the regularized scheme. Note that the Trotter error ϵ of a single rTEBD- L iterative step scales as $\epsilon \sim c_{L/2} \tau^{\frac{L}{2}+1}$ with $c_{L/2}$ the $(L/2)$ th-order coefficient of the BCH series. It turns out that the higher the accuracy required by the outcome, the better the regularized algorithm manifests its superiority of running speed. Take the above $s = 1$ HAF model as an example. Set the Trotter error $\epsilon \sim 10^{-12}$ which is requested by an output with accuracy of 10 \sim 11 digits [say, the rTEBD-4 with $\mathcal{D} = 80$ yields $e_g = -1.401484038(1)$]. Time costs of the rTEBD-4 and rTEBD-6 are reduced to about 1/6 and 1/2, respectively, of that of the rTEBD-2, but the rTEBD-8 is not able to exhibit speedup until the Trotter error $\epsilon \lesssim 10^{-14}$.

Extensions of the regularized scheme to diverse configurations of the 2D lattice systems are highly nontrivial, among which we focus below on the honeycomb lattice to elaborate its superiority. Specifically, we deal with the KHM [50] which is defined by

$$H = \frac{1}{2} \sum_{\langle i,j \rangle_\gamma} J_\gamma \sigma_i^\gamma \sigma_j^\gamma, \quad (5)$$

in which the coupling of any two neighboring sites $\langle i, j \rangle$ is dependent on the direction of their bond $\gamma (= x, y, z)$, as indicated in Fig. 2 (a). By extending the primitive PEPS [28] to a coarse-grained version, we apply the regularized factorization of the projection to obtain the GS at the isotropic points ($J_\gamma = J_{\gamma'} = \pm 1$) where critical gapless spin liquid phases are formed. As the same scheme is applicable to the honeycomb lattice with Heisenberg interactions, the result of the GS of the HAF, $H = \sum_{\langle i,j \rangle} \vec{S}_i \cdot \vec{S}_j$, will also be presented.

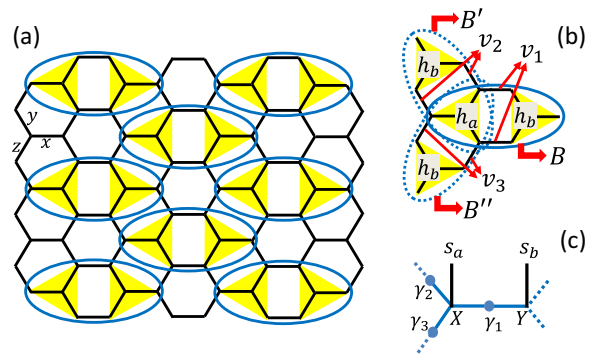


FIG. 2. Schematic figures for the regularized scheme and corresponding rTNS-(4,4) on the 2D honeycomb lattice. (a) Partition of the lattice into 8-site unit cells $\{B\}$ for both the HAF and KHM. The three x , y , and z links are marked out for the KHM [Eq. (5)]. (b) Unit cells $\{B\}$, $\{B'\}$ and $\{B''\}$ along the orientations x , y , and z on which the operators $U_1[B]$, $\bar{U}_2[B']$ and $\bar{U}_3[B'']$ are imposed in turn, respectively. (c) Graphical representation of the rTNS-(4,4), see Eq. (7).

We partition the honeycomb lattice into \mathcal{N}^2 copies of 8-site unit cells $\{B\}$ with $H_B = h_a + v_1 + h_b$. The Hilbert space of each B is indicated by the indices $\{s_a, s_b\}$ with a and b denoting two coarse-grained sublattices [see Fig. 2 (a)]. The total Hamiltonian of the system hence reads $H = \sum_{k=1}^{\mathcal{N}^2} (H_B^{[k]} + v_2^{[k]} + v_3^{[k]})$ where v_2 and v_3 account for the interblock couplings between B 's. The propagator is factorized according to

$$e^{-\tau H} = \bigotimes_{\{B''\}} \bar{U}_3[B''] \times \bigotimes_{\{B'\}} \bar{U}_2[B'] \times \bigotimes_{\{B\}} U_1[B], \quad (6)$$

in which the first layer with $U_1[B] = e^{-\tau H_B}$ denotes the evolution generated by the free Hamiltonian of all \mathcal{N}^2 disconnected B 's. The operators $\bar{U}_2[B']$ and $\bar{U}_3[B'']$ in the second and the third layers [see Fig. 2 (b)] are responsible for the interblock couplings v_2 and v_3 , respectively. They are constructed through the regularized scheme with either the open and or the periodic prescriptions [60]. The corresponding representation of the wave function, referred as rTNS-(4,4), is a coarse-grained version of the PEPS produced by the primitive algorithm [28]:

$$|\Psi\rangle = \sum_{\{s_a, s_b\}} \text{tTr} \prod_{a,b} \gamma_1[B] \gamma_2[B'] \gamma_3[B''] X^{s_a} Y^{s_b} |s_a s_b\rangle \quad (7)$$

where the product is taken over all $2\mathcal{N}^2$ sublattices $\{a, b\}$ and tTr stands for the tensor trace. The tensors X^{s_a} and Y^{s_b} are of rank four, possessing the spin indices $s_{a,b}$ with enlarged dimension 2^4 and three virtual bond indices of dimension \mathcal{D} , and $\gamma_1[B]$, $\gamma_2[B']$ and $\gamma_3[B'']$ are diagonal matrices, related to the singular-value decomposition (SVD) along the three orientations [see Fig. 2 (c)].

We first run the regularized algorithm for the iterative imaginary time evolution incorporating with the simple update method to obtain the GS of the system in the thermodynamic limit. In view of the symmetry of the

TABLE II. GS energies of the pure KHM at isotropic points and the HAF obtained by their rTNS-(4, 4) wave functions with various bond dimensions \mathcal{D} and χ .

KHM				
e_g	$\chi = \mathcal{D}$	$\chi = \frac{3\mathcal{D}-1}{2}$	$\chi = 2\mathcal{D}$	$\chi = 3\mathcal{D}$
$\mathcal{D} = 5$	-0.3871731	-0.3871732	-0.3871732	-0.3871732
$\mathcal{D} = 7$	-0.3896083	-0.3896084	-0.3896084	-0.3896084
$\mathcal{D} = 9$	-0.3902985	-0.3903003	-0.3903004	-0.3903005
$\mathcal{D} = 11$	-0.3909176	-0.3909270	-0.3909290	-0.3909293
HAF				
e_g	$\chi = \mathcal{D}$	$\chi = \frac{3}{5}\mathcal{D}$	$\chi = 2\mathcal{D}$	$\chi = 3\mathcal{D}$
$\mathcal{D} = 6$	-0.54123282	-0.54123284	-0.54123284	-0.54123284
$\mathcal{D} = 8$	-0.54384911	-0.54384959	-0.54384974	-0.54384975
$\mathcal{D} = 10$	-0.54412707	-0.54412974	-0.54413015	-0.54413018
$\mathcal{D} = 12$	-0.54425157	-0.54425354	-0.54425368	-0.54425370

lattice with respect to the spatial 120° -rotation, a three-fold staggered way to perform the operators is exploited for the iteration [60]. We take $\tau = 0.1$ initially and reduce it successively till $\tau = 0.1 \times 2^{-6}$. The randomly generated initial states converge to a stable rTNS-(4, 4) almost in all times, evidenced by the (normalized) singular values of $\gamma_1[B]$, $\gamma_2[B']$ and $\gamma_3[B'']$. The algorithm outputs the same results for the ferromagnetic and anti-ferromagnetic KHMs ($J_\gamma = \pm 1$) including the values of $\gamma_{1,2,3}$ and the GS energy, and their accumulated iteration number should be much larger (~ 20 times or more) than that of the HAF model. On the other hand, the periodic prescription is shown to perform better than the open one, and this becomes dramatic for the KHM with increasing \mathcal{D} : the convergence by the open prescription becomes difficult for the KHM with $\mathcal{D} > 6$, but the periodic one can work for much higher \mathcal{D} .

As has been mentioned previously, the regularized algorithm can reduce two kinds of error, the Trotter decomposition and the approximation of the mean-field-like environment with respect to the simple update. Both these two aspects should play decisive roles in achieving stable convergence for the KHM. This is because that the “evolutionary rate” caused by the imaginary-time propagator of the gapless system is very slow and the tendency toward the optimal target state is easily affected by the two kinds of errors. This is also the reason why the primitive PEPS algorithm fails to obtain satisfactory results: the two-site propagator together with the mean-field-like environment of the simple update scheme is too rough to obtain the strongly correlated spin liquid phase although the Trotter error could be made negligibly small; while in the full update scheme the Trotter error is relatively large as the time cost of the algorithm is very expensive and increases linearly with $1/\tau$.

With the obtained wave function, we can then estimate physical expectation values by applying the contraction algorithm to the full summation over the 2D TN. It turns out that the contraction associated with the rTNS-(4, 4) has desirable convergency, e.g., the boundary MPS method [26] is able to yield sufficient accuracy by taking the bond dimension χ to be $2\mathcal{D} \sim 3\mathcal{D}$. Moreover, a notable physical property of the rTNS-(4, 4) obtained for the KHM is its null magnetization for all \mathcal{D} values shown in Table II ($\langle \sigma_i^z \rangle$ being $10^{-12} \sim 10^{-10}$ attributed to the numerical error), which unambiguously affirms the outputted spin liquid phase. The average values of the GS energy, i.e., $e_g \equiv \frac{1}{8}(\langle H_B \rangle + \langle v_2 \rangle + \langle v_3 \rangle)$ per site or $\frac{2}{3}e_g$ per bond, are shown in Table II for both the KHM and HAF. The outputs of the contraction converge rapidly with χ (slightly slowing down as \mathcal{D} increases). When χ takes the value of $2\mathcal{D} \sim 3\mathcal{D}$, the accuracy of the contraction is already above 10^{-6} or 10^{-7} for the KHM and the HAF, respectively, which is sufficient to warrant the output to be the upper bound of the exact energy. The converged value of $\mathcal{D} = 13$ for the KHM is $e_g = -0.39134$, which is about 0.58% higher than the exact one as the gapless GS energy exhibits algebraic convergence with \mathcal{D} . For the HAF model, the result of $\mathcal{D} = 14$ ($e_g = -0.54432$, attainable by a desktop or laptop) is already comparable to those of the Monte Carlo (-0.54455) [61] and of the second renormalization on the primitive TN state with $\{\mathcal{D}, \chi\} = \{16, 130\}$ (-0.54440) [62, 63], and an accuracy of 10^{-6} ($\mathcal{D} \approx 24$ according to extrapolation) is achievable by the current computing power.

To summarize, the regularized TN algorithm is developed and shown to be able to yield reliable results for both 1D and 2D quantum lattice systems with modest computational resources. As the ability to capture the spin liquid phase is tested by the pure KHM with non-magnetized outputs, further applications of the algorithm to the KHM with competing interactions and to other frustrated models are expected and should be addressed elsewhere. The lattice units we have adopted for the honeycomb lattice assume a simple structure with two sublattices. Proper partitions of the honeycomb and other lattices into unit cells with multiple components will result in regularized TN states with multiple local tensors on which the high-order SVD is suitably applied in order to implement the update. Since the factorization method for the time evolution is applicable to general quantum lattices, systematic analyses and applications of the regularized algorithm to probe the GS as well as the dynamical and thermodynamic properties for varieties of lattice systems, will be a research subject of the next step.

Acknowledgments— This work was supported by the NSFC, China, under Grant No. 12147207.

[1] R. Orús, “Tensor networks for complex quantum systems,” *Nat. Rev.* **1**, 538 (2019).

[2] J.I. Cirac, D. Pérez-García, N. Schuch, and F. Verstraete, “Matrix product states and projected entangled

- pair states: Concepts, symmetries, theorems,” *Rev. Mod. Phys.* **93**, 045003 (2021).
- [3] G. Vidal, “Efficient Simulation of One-Dimensional Quantum Many-Body Systems,” *Phys. Rev. Lett.* **93**, 040502 (2004).
- [4] M.B. Hastings, “Entropy and entanglement in quantum ground states,” *Phys. Rev. B* **76**, 035114 (2007).
- [5] X. Chen, Z.-C. Gu, and X.-G. Wen, “Classification of gapped symmetric phases in one-dimensional spin systems,” *Phys. Rev. B* **83**, 035107 (2011).
- [6] U. Schollwöck, “The density-matrix renormalization group in the age of matrix product states,” *Ann. Phys.* **326**, 96 (2011).
- [7] G. Vidal, “Entanglement Renormalization,” *Phys. Rev. Lett.* **99**, 220405 (2007).
- [8] G. Evenbly and G. Vidal, “Tensor Network Renormalization,” *Phys. Rev. Lett.* **115**, 180405 (2015).
- [9] S. Yang, Z.-C. Gu, and X.-G. Wen, “Loop Optimization for Tensor Network Renormalization,” *Phys. Rev. Lett.* **118**, 110504 (2017).
- [10] M. Bal, M. Mariën, J. Haegeman, and F. Verstraete, “Renormalization Group Flows of Hamiltonians Using Tensor Networks,” *Phys. Rev. Lett.* **118**, 250602 (2017).
- [11] V. Murg, F. Verstraete, and J.I. Cirac, “Exploring frustrated spin systems using projected entangled pair states,” *Phys. Rev. B* **79**, 195119 (2009).
- [12] S. Yan, D. A. Huse, and S. R. White, “Spin-Liquid Ground State of the $S = 1/2$ Kagome Heisenberg Antiferromagnet,” *Science* **332**, 1173 (2011).
- [13] F. Mezzacapo and M. Boninsegni, “Ground-state phase diagram of the quantum $J_1 - J_2$ model on the honeycomb lattice,” *Phys. Rev. B* **85**, 060402(R) (2012).
- [14] H.J. Liao, Z.Y. Xie, J. Chen, X.J. Han, H.D. Xie, B. Normand, and T. Xiang, “Heisenberg Antiferromagnet on the Husimi Lattice,” *Phys. Rev. B* **93**, 075154 (2016).
- [15] T. Picot, M. Ziegler, R. Orús, and D. Poilblanc, “Spin- S Kagome Quantum Antiferromagnets in a Field with Tensor Networks,” *Phys. Rev. B* **93**, 060407(R) (2016).
- [16] S.R. White, “Density Matrix Formulation for Quantum Renormalization Groups,” *Phys. Rev. Lett.* **69**, 2863 (1992).
- [17] S.R. White, “Density-matrix algorithms for quantum renormalization groups,” *Phys. Rev. B* **48**, 10345 (1993).
- [18] S. Östlund and S. Rommer, “Thermodynamic Limit of Density Matrix Renormalization,” *Phys. Rev. Lett.* **75**, 3537 (1995).
- [19] G. Vidal, “Classical Simulation of Infinite-Size Quantum Lattice Systems in One Spatial Dimension,” *Phys. Rev. Lett.* **98**, 070201 (2007).
- [20] R. Orús and G. Vidal, “Infinite time-evolving block decimation algorithm beyond unitary evolution,” *Phys. Rev. B* **78**, 155117 (2008).
- [21] C.V. Kraus, N. Schuch, F. Verstraete, and J.I. Cirac, “Fermionic Projected Entangled Pair States,” *Phys. Rev. A* **81**, 052338 (2010).
- [22] P. Corboz, R. Orús, B. Bauer, and G. Vidal, “Simulation of Strongly Correlated Fermions in Two Spatial Dimensions with Fermionic Projected Entangled-Pair States,” *Phys. Rev. B* **81**, 165104 (2010).
- [23] D. Poilblanc, P. Corboz, N. Schuch, and J.I. Cirac, “Resonating-Valence-Bond Superconductors with Fermionic Projected Entangled Pair States,” *Phys. Rev. B* **89**, 241106(R) (2014).
- [24] N. Bultinck, D.J. Williamson, J. Haegeman, and F. Verstraete, “Fermionic Matrix Product States and One-Dimensional Topological Phases,” *Phys. Rev. B* **95**, 075108 (2017).
- [25] F. Verstraete and J.I. Cirac, “Renormalization Algorithms for Quantum-Many Body Systems in Two and Higher Dimensions,” arXiv: cond-mat/0407066.
- [26] J. Jordan, R. Orús, G. Vidal, F. Verstraete, and J.I. Cirac, “Classical Simulation of Infinite-Size Quantum Lattice Systems in Two Spatial Dimensions,” *Phys. Rev. Lett.* **101**, 250602 (2008).
- [27] Z.Y. Xie, J. Chen, J.F. Yu, X. Kong, B. Normand, and T. Xiang, “Tensor Renormalization of Quantum Many-Body Systems Using Projected Entangled Simplex States,” *Phys. Rev. X* **4**, 011025 (2014).
- [28] H.C. Jiang, Z.Y. Weng, and T. Xiang, “Accurate Determination of Tensor Network State of Quantum Lattice Models in Two Dimensions,” *Phys. Rev. Lett.* **101**, 090603 (2008).
- [29] P. Czarnik, L. Cincio, and J. Dziarmaga, “Projected Entangled Pair States at Finite Temperature: Imaginary Time Evolution with Ancillas,” *Phys. Rev. B* **86**, 245101 (2012).
- [30] L. Vanderstraeten, J. Haegeman, P. Corboz, and F. Verstraete, “Gradient Methods for Variational Optimization of Projected Entangled-Pair States,” *Phys. Rev. B* **94**, 155123 (2016).
- [31] P. Czarnik, J. Dziarmaga, and P. Corboz, “Time Evolution of an Infinite Projected Entangled Pair State: An Efficient Algorithm,” *Phys. Rev. B* **99**, 035115 (2019).
- [32] P.W. Anderson, “The Resonating Valence Bond State in La_2CuO_4 and Superconductivity,” *Science* **235**, 1196 (1987).
- [33] N. Read and S. Sachdev, “Large- N Expansion for Frustrated Quantum Antiferromagnets,” *Phys. Rev. Lett.* **66**, 1773 (1991).
- [34] J.B. Marston and C. Zeng, “Spin-Peierls and Spin-Liquid Phases of Kagome Quantum Antiferromagnets,” *J. Appl. Phys.* **69**, 5962 (1991).
- [35] R. Moessner and S. L. Sondhi, “Resonating Valence Bond Phase in the Triangular Lattice Quantum Dimer Model,” *Phys. Rev. Lett.* **86**, 1881 (2001).
- [36] X.-G. Wen, “Quantum Orders and Symmetric Spin Liquids,” *Phys. Rev. B* **65**, 165113 (2002).
- [37] M.R. Norman, “Colloquium: Herbertsmithite and the Search for the Quantum Spin Liquid,” *Rev. Mod. Phys.* **88**, 041002 (2016).
- [38] O.A. Starykh and L. Balents, “Dimerized Phase and Transitions in a Spatially Anisotropic Square Lattice Antiferromagnet,” *Phys. Rev. Lett.* **93**, 127202 (2004).
- [39] H.-H. Hung, C.-D. Gong, Y.-C. Chen, and M.-F. Yang, “Search for Quantum Dimer Phases and Transitions in a Frustrated Spin Ladder,” *Phys. Rev. B* **73**, 224433 (2006).
- [40] T. Hikihara and O.A. Starykh, “Phase Diagram of the Frustrated Spin Ladder,” *Phys. Rev. B* **81**, 064432 (2010).
- [41] G. Barcza, Ö. Legeza, R.M. Noack, and J. Solyom, “Dimerized Phase in the Cross-Coupled Antiferromagnetic Spin Ladder,” *Phys. Rev. B* **86**, 075133 (2012).
- [42] P. Nikolic and T. Senthil, “Physics of Low-Energy Singlet States of the Kagome Lattice Quantum Heisenberg Antiferromagnet,” *Phys. Rev. B* **68**, 214415 (2003).
- [43] R.R.P. Singh and D.A. Huse, “Ground State of the Spin-1/2 Kagome-Lattice Heisenberg Antiferromagnet,” *Phys.*

- Rev. B **76**, 180407(R) (2007).
- [44] H.-C. Jiang, Z.-Y. Weng, and D.N. Sheng, “Density Matrix Renormalization Group Numerical Study of the Kagome Antiferromagnet,” *Phys. Rev. Lett.* **101**, 117203 (2008).
- [45] G. Evenbly and G. Vidal, “Frustrated Antiferromagnets with Entanglement Renormalization: Ground State of the Spin-1/2 Heisenberg Model on a Kagome Lattice,” *Phys. Rev. Lett.* **104**, 187203 (2010).
- [46] S. Depenbrock, I.P. McCulloch, and U. Schollwöck, “Nature of the Spin-Liquid Ground State of the $S = 1/2$ Heisenberg Model on the Kagome Lattice,” *Phys. Rev. Lett.* **109**, 067201 (2012).
- [47] Y. Iqbal, F. Becca, S. Sorella, and D. Poilblanc, “Gapless spin-liquid phase in the kagome spin-1/2 Heisenberg antiferromagnet,” *Phys. Rev. B* **87**, 060405(R) (2013).
- [48] H.J. Liao, Z.Y. Xie, J. Chen, Z.Y. Liu, H.D. Xie, R.Z. Huang, B. Normand, and T. Xiang, “Gapless Spin-Liquid Ground State in the $S = 1/2$ Kagome Antiferromagnet,” *Phys. Rev. Lett.* **118**, 137202 (2017).
- [49] J.-W. Mei, J.-Y. Chen, H. He, and X.-G. Wen, “Gapped spin liquid with z_2 topological order for the kagome Heisenberg model,” *Phys. Rev. B* **95**, 235107 (2017).
- [50] A. Kitaev, “Anyons in an exactly solved model and beyond,” *Ann. Phys. (Amsterdam)* **321**, 2 (2006).
- [51] J. Chaloupka, G. Jackeli, and G. Khaliullin, “Kitaev-Heisenberg Model on a Honeycomb Lattice: Possible Exotic Phases in Iridium Oxides A_2IrO_3 ,” *Phys. Rev. Lett.* **105**, 027204 (2010).
- [52] I. Kimchi and Y.-Z. You, “Kitaev-Heisenberg- J_2 - J_3 model for the iridates A_2IrO_3 ,” *Phys. Rev. B* **84**, 180407(R) (2011).
- [53] J. OsorioIregui, P. Corboz, and M. Troyer, “Probing the stability of the spin-liquid phases in the Kitaev-Heisenberg model using tensor network algorithms,” *Phys. Rev. B* **90**, 195102 (2014).
- [54] M. Gohlke, G. Wachtel, Y. Yamaji, F. Pollmann, and Y.B. Kim, “Quantum spin liquid signatures in Kitaev-like frustrated magnets,” *Phys. Rev. B* **97**, 075126 (2018).
- [55] S.-S. Zhang, G.B. Halász, W. Zhu, and C.D. Batista, “Variational study of the Kitaev-Heisenberg-Gamma model,” *Phys. Rev. B* **104**, 014411 (2021).
- [56] H.-Y. Lee, R. Kaneko, T. Okubo, and N. Kawashima, “Gapless Kitaev Spin Liquid to Classical String Gas through Tensor Networks,” *Phys. Rev. Lett.* **123**, 087203 (2019).
- [57] M. Suzuki, “Fractal decomposition of exponential operators with applications to many-body theories and Monte-Carlo simulations,” *Phys. Lett. A* **146**, 319 (1990).
- [58] Z.Y. Xie, H.J. Liao, R.Z. Huang, H.D. Xie, J. Chen, Z.Y. Liu, and T. Xiang, “Optimized contraction scheme for tensor-network states,” *Phys. Rev. B* **96**, 045128 (2017).
- [59] Similar prescriptions have been proposed in the regularized numerical renormalization group in which the pair of block Hamiltonians are exploited to construct basis states for the compound lattice, see L.-X. Cen, “Revisiting numerical real-space renormalization group for quantum lattice systems,” *Ann. Phys.* **397**, 151 (2018).
- [60] See Appendix for the detailed demonstration of the regularized prescription, its generalization for the honeycomb lattice and the corresponding three-fold staggered iteration.
- [61] U. Löw, “Properties of the two-dimensional spin-1/2 Heisenberg model on a honeycomb lattice with interlayer coupling,” *Condens. Matter Phys.* **12**, 497 (2009).
- [62] Z.Y. Xie, H.C. Jiang, Q.N. Chen, Z.Y. Weng, and T. Xiang, “Second Renormalization of Tensor-Network States,” *Phys. Rev. Lett.* **103**, 160601 (2009).
- [63] H.H. Zhao, Z.Y. Xie, Q.N. Chen, Z.C. Wei, J.W. Cai, and T. Xiang, “Renormalization of tensor-network states,” *Phys. Rev. B* **81**, 174411 (2010).

Appendix A: Regularized factorization of the propagator and the limited order of the BCH expansions

In order to explain the rationality for the factorization of the propagator shown in Eqs. (1)-(3), we first reveal that the combining operator $e^{-\tau H}e^{\tau H_0}$ given in Eq. (4) possesses an effective piece-wise structure. To this end, one applies the BCH expansion

$$e^{-\tau H}e^{\tau H_0} = e^{-\tau\tilde{V}_1 - \frac{\tau^2}{2}\tilde{V}_2 + \frac{\tau^3}{12}\tilde{V}_3 + \dots}, \quad (\text{A1})$$

in which \tilde{V}_i 's contained in the first three terms of the exponential read as

$$\tilde{V}_1 = H - H_0 = \sum_k v^{k,k+1} \equiv \sum_k \tilde{v}_1^{[k]}, \quad (\text{A2})$$

$$\tilde{V}_2 = [H, H_0] = \sum_k [v^{k,k+1}, H_0] \equiv \sum_k \tilde{v}_2^{[k]}, \quad (\text{A3})$$

$$\tilde{V}_3 = \sum_k [H + H_0, [v^{k,k+1}, H_0]] \equiv \sum_k \tilde{v}_3^{[k]}. \quad (\text{A4})$$

Truncation to the first term of the above BCH series yields simply the conventional Trotter-Suzuki decomposition. It is crucial to note that the commutation and the corresponding nestings involving $v^{k,k+1}$ in high-order terms will expand the range of the coupling (e.g., for the case that H involves only the nearest-neighboring interaction, it widens two more sites by increasing each order of the expansion) before it overlaps the adjacent ones. To guarantee the effective piece-wise structure of the operator, the length L of the block and the expanding order n of the BCH series should satisfy $L/2 \geq n$, e.g., for the case of the nearest-neighboring interaction. This is clearly seen from the fact that the term $V^{k,k+1}$ in Eq. (4) can be expressed explicitly as

$$V^{k,k+1} = \tau\tilde{v}_1^{[k]} + \frac{\tau^2}{2}\tilde{v}_2^{[k]} - \frac{\tau^3}{12}\tilde{v}_3^{[k]} + \dots, \quad (\text{A5})$$

in which all $\tilde{v}_n^{[k]}$'s ($n = 1, \dots, L/2$) are of local form, e.g.,

$$\tilde{v}_1^{[k]} = v^{k,k+1}, \quad (\text{A6})$$

$$\tilde{v}_2^{[k]} = [\tilde{v}_1^{[k]}, h_r^{[k]} + h_l^{[k+1]}], \quad (\text{A7})$$

$$\tilde{v}_3^{[k]} = [2h_r^{[k]} + 2h_l^{[k+1]} + v^{k,k+1}, \tilde{v}_2^{[k]}]. \quad (\text{A8})$$

As the range of every $V^{k,k+1}$ is limited by the expanding order, the condition $L/2 \geq n$ warrants that $V^{k,k+1}$ is local and satisfies $[V^{k,k+1}, V^{k',k'+1}] = 0$.

To demonstrate the validity of the decomposition one then needs only to show that every piece of the operator, $e^{-V^{k,k+1}}$, can be efficiently simulated by the two prescriptions of $\tilde{U}_L(\tau)$ presented in Eq. (2) and (3), alternatively. This can be recognized directly by expanding them via the BCH formula, both of which give rise to

$$\tilde{U}_L(\tau) = e^{-\tau v_{lr} - \frac{\tau^2}{2}[v_{lr}, h_l + h_r] + \frac{\tau^3}{12}[2h_l + 2h_r + v_{lr}, [v_{lr}, h_l + h_r]] + \dots} \quad (\text{A9})$$

Under the restriction of the expanding order $n \leq L/2$, the above expression reproduces exactly the one of $e^{-V^{k,k+1}}$ except for a translation of $L/2$ sites.

In the decomposing scheme of Eq. (1), we have set the ingredient of the propagator generated by the free Hamiltonian term to be the first layer. On the contrary, an alternative way to decompose the propagator can also be given by rewriting Eq. (4) as

$$\begin{aligned} e^{-\tau H} &= e^{-\tau H_0} e^{\tau H_0} e^{-\tau H} \\ &= e^{-\tau H_0} \times e^{-\sum_{k=1}^N \tilde{V}^{k,k+1}}, \end{aligned} \quad (\text{A10})$$

in which $\tilde{V}^{k,k+1}$, yielded by the BCH expansion of $e^{\tau H_0}e^{-\tau H}$, possesses a similar local structure with $V^{k,k+1}$ shown in Eq. (A5). It thus leads to

$$e^{-\tau H} = [U_L(\tau)]^{\otimes \mathcal{N}} \times [\tilde{U}_L(\tau)]^{\otimes \mathcal{N}}. \quad (\text{A11})$$

The corresponding open and periodic prescriptions to construct $\tilde{U}_L(\tau)$ are given by

$$\tilde{U}_L^{(1)}(\tau) = e^{\tau(h_l + h_r)} e^{-\tau H_L} \quad (\text{A12})$$

and

$$\tilde{U}_L^{(2)}(\tau) = e^{\tau H_L^\ominus} e^{-\tau H_L^p}, \quad (\text{A13})$$

respectively. That is to say, the factorization scheme of Eq. (A11) exchanges the order of the two layers of the operations indicated in Eq. (1) and the associated prescriptions (2) and (3) responsible for the interblock coupling should also change the order of their generating operators accordingly [cf. expressions of $\tilde{U}_L^{(1,2)}(\tau)$ presented in Eqs. (2) and (3)]. At this stage, a different version of the staggered way to implement the action of $e^{-\tau H}$ for the iteration, i.e., via the decomposition of Eq. (1) at every odd time and via that of Eq. (A11) at every even time, is suggested. Since it adopts a distinct strategy from that shown in Fig. 1(b), a compatible iterative scheme can be designed by combining these two staggered strategies, via which the Trotter error can be further suppressed.

Appendix B: Regularized factorization and staggered iteration for the honeycomb lattice

Since the Hamiltonians utilized in the open prescription to construct the propagator are clear themselves, we illustrate here the Hamiltonians with connected boundary which are employed by the periodic prescription to construct the propagator. By choosing the lattice units $\{B\}$ for the free Hamiltonian $H_0 = \sum_{k=1}^{\mathcal{N}^2} H_B^{[k]}$, one needs to construct $\tilde{U}_2[B']$ and $\tilde{U}_3[B'']$ for the factorization shown in Eq. (6). The periodic prescription for $\tilde{U}_2[B']$ exploits a block Hamiltonian with periodic boundary condition $H_B^p = H_B + v_2 + v_3$ (noticing $H_{B'}^p = H_{B''}^p = H_B^p$, see Fig. 3) and the other one by subtracting the term v_2 from H_B^p : $H_{B'}^\ominus = H_B^p - v_2$, that is,

$$\tilde{U}_2[B'] = e^{-\tau H_{B'}^p} e^{\tau H_{B'}^\ominus}. \quad (\text{B1})$$

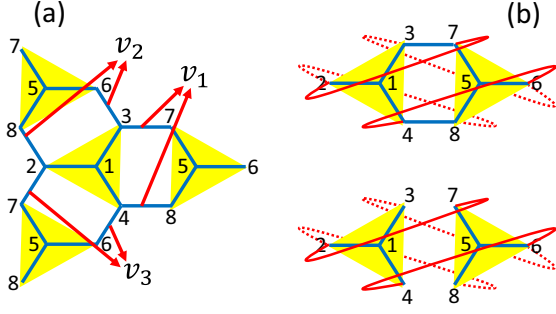


FIG. 3. Schematic figures of the block Hamiltonians employed to construct the propagator in the regularized TN algorithm. (a) An example to mark the order of sites in the lattice units. (b) The pair of block Hamiltonians with connected boundary, $H_B^p = H_B + v_2 + v_3$ (upper panel) and $H_B^o = H_B^p - v_1$ (bottom panel), with which the operator $\bar{U}_1[B]$ is constructed.

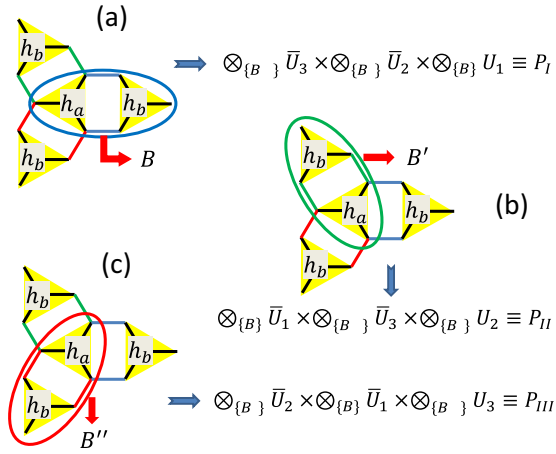


FIG. 4. Schematic figures of the three different “gate” sequences to simulate the propagator generated by the honeycomb lattice system. The notations P_I , P_{II} and P_{III} are introduced to specify them of (a), (b) and (c) which relate to each other by a 120° spatial rotation in turn.

The operator $\bar{U}_3[B'']$ is constructed similarly

$$\bar{U}_3[B''] = e^{-\tau H_{B''}^p} e^{\tau H_{B''}^o}, \quad (\text{B2})$$

in which $H_{B''}^o = H_{B''}^p - v_3$.

Concerning the symmetry of the lattice with respect to the spatial 120° -rotation, one can also choose the lattice units $\{B'\}$ or $\{B''\}$ as the free Hamiltonian, i.e., $H_0 = \sum_{k=1}^{\mathcal{N}^2} H_{B'}^{[k]}$ or $H_0 = \sum_{k=1}^{\mathcal{N}^2} H_{B''}^{[k]}$. Accordingly, the decomposition of the propagator $e^{-\tau H}$ can be realized by the following two different “gate” sequences

$$e^{-\tau H} = \bigotimes_{\{B\}} \bar{U}_1[B] \times \bigotimes_{\{B''\}} \bar{U}_3[B''] \times \bigotimes_{\{B'\}} U_2[B'], \quad (\text{B3})$$

$$e^{-\tau H} = \bigotimes_{\{B'\}} \bar{U}_2[B'] \times \bigotimes_{\{B\}} \bar{U}_1[B] \times \bigotimes_{\{B''\}} U_3[B'']. \quad (\text{B4})$$

Here, $U_2[B']$ and $U_3[B'']$ in the first layer of the two sequences are just the propagators generated by the two free Hamiltonians defined on $\{B'\}$ and $\{B''\}$, respectively. The operator $\bar{U}_1[B]$ is responsible for the coupling v_1 and is constructed via $\bar{U}_1[B] = e^{-\tau H_B^p} e^{\tau H_B^o}$ with $H_B^o = H_B^p - v_1$. These three different gate sequences to simulate $e^{-\tau H}$, i.e., indicated by Eqs. (6), (B3) and (B4), relate to each other by a 120° spatial rotation in turn and are shown schematically in Fig. 4 with the notations P_I , P_{II} and P_{III} , respectively. In analogy to the staggered iteration previously proposed for the 1D lattice system (cf. Fig. 1), a 3-fold staggered way to apply these gate sequences can be devised to implement the iteration in the regularized TN algorithm, which is helpful to reduce further the error of the factorization and restore the 120° rotational symmetry for the honeycomb lattice.

In the practical performance of the iteration, these three sequences of gate operations are implemented following the order of P_I , then P_{III} , and P_{II} last. The benefit of doing so is that the consecutive twice operations imposed on the same lattice units, e.g., $\bar{U}_3[B'']$ in the last layer of P_I and $U_3[B'']$ in the first layer of P_{III} that are imposed on the same $\{B''\}$, can be merged, which is able to save 1/3 of the iteration times.